DOI: 10.1021/ma9022229

Macromolecules
ARTICLE

Phase Transitions of Block Copolymer Film on Homopolymer-Grafted Substrate

Hyungju Ahn,[†] Changhak Shin, Byeongdu Lee,*[,‡] and Du Yeol Ryu*[,†]

[†]*Department of Chemical and Biomolecular Engineering, Yonsei University, 134 Sinchon-dong, Seodaemun-gu, Seoul 120-749, Korea and* [‡]*X-ray Science Division, Advanced Photon Source, Argonne National Laboratory, 9700 S. Cass Ave., Argonne, Illinois 60439*

Received October 12, 2009; Revised Manuscript Received December 15, 2009

ABSTRACT: Morphological transitions such as the order-to-order transition (OOT) and the order-to-disorder transition (ODT) for an asymmetric polystyrene-*block*-polyisoprene (PS-*b*-PI) were investigated in bulk and film. The PS-rich block copolymer (BCP) bulk possessed the lamella morphology (LAM), which transformed to the gyroid (GYR) and then disordering (DIS) with increasing temperature. Between the LAM and GYR, a perforated layered structure (PL) and phase mixture (*Fddd* + GYR) of poorly ordered *Fddd* and GYR were observed. On the other hand, the film coated on a PS-grafted substrate showed a phase transition from random LAM to epitaxially oriented hexagonally modulated layer (HML) morphology. The HML transformed to GYR with further increasing temperature. The *Fddd* morphology observed in bulk was not observed at any stage of phase transitions in the film. The BCP film presented not only different OOT pathway but also higher OOT and ODT temperatures. In addition, the *d*-spacings of layers parallel to a substrate were not decreased at all with increasing temperature except when there was a structural transition, suggesting no relaxation of stretched BCP chains that are normal to the film. These results may be correlated dominantly to the interfacial energy between PS block of BCP and PS brushes on a substrate, which suppresses the compositional fluctuation of BCP in the film especially along the film normal direction, leading to anisotropic variation of *d*-spacings.

Introduction

Block copolymer (BCP) has attracted great attention due to the growing interest for advanced and efficient technologies in various applications such as microelectronic engineering and bioengineering,[1−13] while there are still competitive methods in the fields of electron beam lithography, X-ray lithography, and imprinting method. BCP consisting of chemically different two polymers linked covalently allows us to fabricate various nanoscopic patterns and scaffolds, since it can self-assemble into the ordered arrays such as lamellar (LAM), cylindrical (HEX), and spherical (BCC) morphologies, where the morphologies depend on the volume fraction of one component (f), the degree of polymerization (N), and the Flory−Huggins interaction parameter (χ).[14−23] The complex morphologies, like the gyroid (GYR)[20−27] and hexagonally perforated layers (HPL),[27,28] can be observed in the melt state at a narrow range of f and the product of χN. In addition to those, noncubic network phase, designated as *Fddd*, was recently reported by Takenaka et al., which motivates efforts to find new morphology in the BCP melts.[29−31]

A polystyrene-*block*-polyisoprene copolymer (PS-*b*-PI) has been used as a model system to figure out the underlying physics of BCP melt[22−24,29−31] and film[32−34] involving the morphological transition so-called the order-to-order transition (OOT) because it possesses a strong temperature dependence of χ, demonstrating the discrete phase transitions with thermal energy. At a specific composition region from 0.6 to 0.7 of PI volume fraction, it especially presents a sequence of OOT with temperature, in which most results have been well agreed with theoretical considerations by the mean-field approach.[17,18,35]

*To whom correspondence should be addressed: e-mail dyryu@yonsei.ac.kr (D.Y.R.); blee@anl.gov (B.L.).

For the BCP films, the interfacial interactions at film/substrate and film/air interfaces significantly influence not only the microdomain orientation with respect to a substrate but also the phase behavior. Previously we reported that the order-to-disorder transition (ODT) temperature (T_{ODT}) in BCP films is thickness- and substrate-dependent. For the lamella-forming PS-*b*-PI that were coated on PS-grafted substrates and bare Si wafers, where the former and latter substrates preferentially interact respectively with the PS and PI blocks of the BCP, T_{ODT}'s in the films thinner than $12L_0$ (L_0: lamellar period) were significantly higher than that in bulk regardless of substrate type, and they gradually decreased as the film thickness increased and reached plateaus at the film thickness $12L_0$. While the T_{ODT} at plateau in the film on a PS grafted substrate was still higher than that in bulk, the plateau T_{ODT} in the film on bare Si wafer became almost identical to that in bulk.[36] The T_{OOT} (the OOT temperature) and OOT pathway in films have also been shown different from those in bulk. For an asymmetric PS-*b*-PI presenting a sequential phase transition of LAM-HPL-GYR-HEX-DIS (disordering) in the bulk melt, even the weak surface interaction between PI block and a bare Si wafer influences the mesophasic stability in the BCP film, leading to the shift of T_{OOT}'s toward higher temperature and a loss of HEX morphology in the OOT sequence.[34]

More recently, the ODT behavior of a polystyrene-*b*-poly(methyl methacrylate) (PS-*b*-PMMA) coated on a PS-grafted substrate was studied and compared to that of PS-*b*-PI coated on the same type of substrate. The PS-*b*-PMMA film also presented higher T_{ODT} than that in bulk, and its T_{ODT} gradually decreased as the thickness of film increased. T_{ODT} of PS-*b*-PMMA film, however, showed a gentler dependence on the film thickness than those of PS-*b*-PI. This was attributed to the fact that χ of PS-*b*-PMMA is less temperature dependent than that of PS-*b*-PI.[37]

 Published on Web 01/25/2010

In this study we report on the morphological transition of an asymmetric PS-*b*-PI in bulk and film where its PS block is a major component and has the preferential interaction with a PS grafted substrate. Different from the sequential phase transition pathway in the bulk melt, LAM-PL-(*Fddd*+GYR)-GYR-DIS, a hexagonally modulated lamella (HML) structure, is identified in the film, leading to the phase transition pathway in the film, LAM-HML-GYR-DIS. In addition, we discuss that higher OOT and ODT temperatures in the film than those in bulk are not due to the kinetics or slow dynamics but due to the surface and interfacial energy. The decrease of *d*-spacing that is observed for bulk PS-*b*-PI with increasing temperature due to the decrease of χ is not found in films, especially for the *d*-spacing of layers parallel to a substrate. This supports the suppressed compositional fluctuation in BCP film caused by the surface and interfacial energy.

Experimental Section

An asymmetric BCP composed of styrene and isoprene, hereafter denoted as SI-27, was synthesized by the sequential anionic polymerization in cyclohexane at 45 °C under purified argon using *sec*-butyllithium as an initiator. The number-average molecular weight (M_n) and polydispersity index (PDI = M_w/M_n), characterized by size-exclusion chromatography (SEC), were measured to be 26 800 g/mol and 1.06, respectively. PS volume fraction (f_{PS}) of BCP was determined to be 0.617 by ^{1}H nuclear resonance (^{1}H NMR) based on the mass densities of two components (1.05 and 0.90 g/cm^3 for PS and PI). A hydroxyl-terminated polystyrene (M_n = 10 000 g/mol and PDI = 1.09), purchased from Polymer Source Inc., was used to prepare a selectively preferential PS grafted substrate by the simple thermal annealing and rinsing with toluene to remove the nonanchored chains (graft-to method), hence producing a PS brush thickness of 5.0 ± 0.3 nm by ellipsometry (SE MG-1000, Nanoview Co.). BCP film of 657 nm corresponding to $30L_0$ ($L_0 = 2\pi/q^*$) was spin-coated from polymer solution (in toluene) onto the PS-grafted substrate. Subsequently, the thin film was annealed at 110 °C under vacuum for 48 h to allow the chain mobility sufficiently between the glass transition temperature (T_g < 100 °C) of PS block and the first OOT.

Synchrotron scattering experiments were conducted at 4C1 (SAXS) and 4C2 (GISAXS) beamlines at the Pohang Light Source (PLS), Korea. The operating conditions for GISAXS were set to a wavelength of 1.38 Å and the sample-to-detector distance of 2.3 m. The film samples were mounted on a heating cell under vacuum, and the incident angle was set at 0.18°, which is between the critical angle of BCP thin films (0.134°) and the silicon substrate (0.198°). 2D GISAXS patterns were recorded using a CCD detector (Princeton Instruments) positioned at the end of a vacuum guide tube. SAXS was employed to determine the bulk behavior of the BCP with a beam size of 1 × 1 mm^2, a sample-to-detector distance of 2 m, and an exposure time of 60 s under the nitrogen flow to avoid thermal degradation of polymer sample. Both heating experiments for the bulk and film were automatically controlled with a PID temperature controller from 100 to 210 °C at a heating rate of 0.7 and 0.5 °C/min, respectively, and with the exposure time of 60−120 s.

Result and Discussion

SAXS intensity profiles for the bulk SI-27, measured with increasing temperatures at a rate of 0.7 °C/min from 100 to 210 °C after thermally annealing at 110 °C for 48 h under vacuum to allow sufficient chain mobility, are shown in Figure 1 as a function of the scattering vector (q), where $q = (4\pi/\lambda)\sin\theta$; 2θ and λ are the scattering angle and wavelength, respectively. A lamellar (LAM) morphology is observed at low temperature T = 100 °C. Positions of two distinct sharp peaks are integer multiples of the first-order scattering peak position, q^*, which is directly

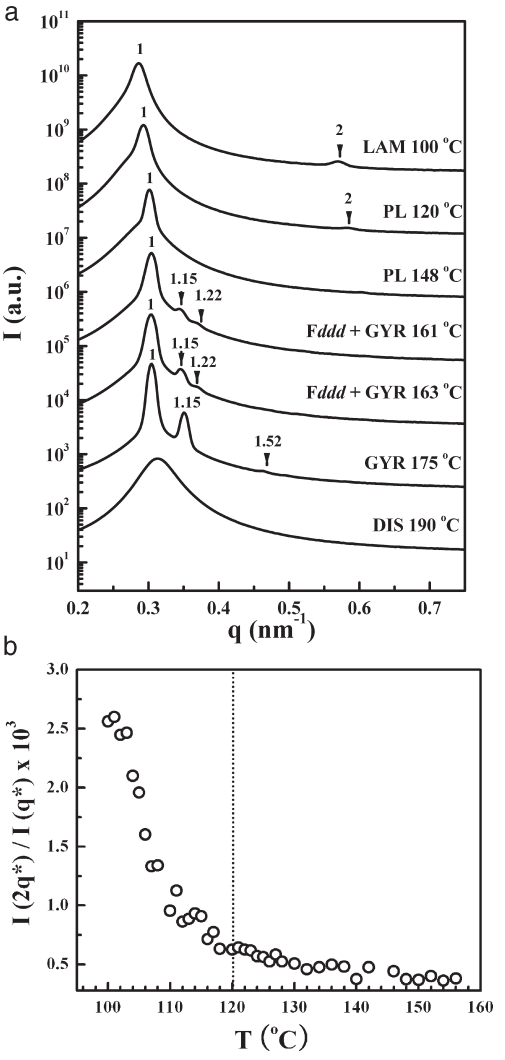

Figure 1. (a) SAXS intensity profiles for the bulk SI-27 as a function of scattering vector (q) at various temperature range from 100 to 190 °C at a heating rate of 0.7 °C/min. To avoid overlapping, the intensity profiles are vertically shifted by a factor of 15. The denoted numbers indicate the scattering vector ratios of q/q^* relative to a primary peak located at q^* (at maximum). (b) Intensity ratio of $2q^*$ peak relative to q^* peak.

related to the conformational status of BCP chains forming LAM. For T = 120 and 148 °C, a shoulder peak at lower q than q^* and the diminishing intensity at $2q^*$ peak position indicate a perforated lamellar (PL) structure (detailed discussion will follow). With a further increase of temperature a new set of diffraction peaks is observed at narrow temperature range between T = 161 and 163 °C. Its three major peaks at q^*, $1.15q^*$ and $1.22q^*$ are not consistent to any single typical BCP morphology known so far. Soon after, the $1.22q^*$ peak disappears, leading to a clear diffraction pattern of the gyroid (GYR) phase for T = 175 °C.

There are several reports on various bulk BCPs such as PI-rich PS-*b*-PI,[24] PEP-rich poly(ethylenepropylene)-*block*-polydimethylsiloxane (PEP-*b*-PDMS),[38] PEO-rich poly(ethylene oxide)-*block*-polyethylethylene (PEO-*b*-PEE),[38] and PEO-based oligomeric BCP surfactant in aqueous solution,[39] illustrating that the direct transition from LAM to GYR is suppressed by the mismatch in the *d*-spacing of epitaxially related lattice planes of the LAM 001 and the GYR 121, as is found in our case as well (see the difference of q^* peak position at T = 100 °C and T = 175 °C). This mismatch would prohibit the GYR grain growth in the LAM phase. In order for the LAM phase to transform to the GYR, the *d*-spacing of LAM needs to be reduced by forming a perforated

layered structure that will be designated as PL, where the perforated channels do not necessarily possess a hexagonal arrangement in a layer plane:[38] $d_{PL} \sim 0.92 d_{LAM}$ for typical materials. In this work we adapt a broader definition of PL: depending on the shape and arrangement of perforated channels, it could be either HPL (hexagonally perforated layer, space group $R\bar{3}m$), HCP (hexagonally close packed structure, space group $P63/mmc$), or HML (hexagonally modulated lamella, space group $C2mm$). The former two cases have hexagonally arranged PS perforations in PI layers, and the last one has undulations in PS layers. When the orderings of perforated or undulation channels in the layer plane are poor, their diffraction patterns for the three structures are similar to that of LAM. In this work two direct evidence for PL are found in SAXS analysis: The first is the abnormally fast increase of q^* with increasing temperature (see Figure 4a). A power-law behavior of $q^* \sim T^{0.33}$ has known for LAM in the bulk PS-*b*-PI.[14] Meanwhile, we observed $q^* \sim T^{0.53}$. Keeping in mind that *d*-spacing can change due to not only the thermodynamic origin such as chain conformation change but also the structural transformation such as the formation of perforated channels, this faster increase of q^* (or decrease of *d*-spacing) supports a gradual perforation that diminishes the thickness of PS layer. Second evidence is a significant decrease in intensity of $2q^*$ peak with increasing temperature as shown in Figure 1b, indicating that thicknesses of two sublayers of PS and PI become identical to each other. The transition temperature from LAM to PL is ~120 °C in our experiment as is determined by the fast drop of the intensity ratio $I(2q^*)/I(q^*)$. Along with these two evidences, it is notable that fwhm (Δq) of q^* peak shown in Figure 4a becomes sharper as LAM transform to PL, suggesting that either the number or width of layers in a domain increases.

Nonetheless, three peaks observed at 160−163 °C cannot be assigned to HPL nor HCP. Recently, a new morphology, the orthorhombic *Fddd*, has been found in PI-rich PS-*b*-PI having a volume fraction near the phase boundary between LAM and GYR. According to Takenaka et al., the second-order peak at $1.22q^*$ indicates the orthorhombic *Fddd*.[29−31] Hence, it is reasonable to assign this morphology to a mixture of *Fddd* and GYR although their higher-order peaks are not found. It should be pointed that *Fddd* has been found at the PS-rich phase and has never been reported in the PI-rich phase yet except for this work. Not only *Fddd*, ordering of GYR in the mixed state is also much poorer compared to that of the well-developed GYR at 175 °C regarding the relative intensity of its second- and higher-order diffraction peaks at $1.15q^*$ and $1.52q^*$, respectively.

At higher temperature (T = 190 °C), the primary scattering peak weakens and broadens abruptly, and higher-order peaks disappear, which is a characteristic correlation hole scattering pattern of a phase-mixed (or disordered) BCP at ODT.[40] Consequently, sequential phase transition LAM-PL-(*Fddd* + GYR)-GYR-DIS phases are observed in the bulk SI-27, which will be compared to those in the film as is presented in Figure 4.

Figure 2 shows 2D GISAXS patterns from the BCP film of thickness 657 ± 7 nm coated on a PS grafted substrate, which were taken with increasing temperature after thermally annealing the thin film at 110 °C for 48 h under vacuum. The sample thickness corresponds to $\sim 30L_0$, where L_0 (or $d = 2\pi/q^*$) is 22.0 nm at 100 °C. In the grazing incidence scattering, q_{xy} and q_z are the in-plane and out-of-plane components of the scattering vector q, respectively. They are normal to the plane of incidence and to the sample surface, respectively. Incident angle (α_i) was set to 0.18° to probe the internal film structures; the critical angle (α_c) and electron density of SI-27 are about 0.134° and 0.322 e/Å^3, respectively.

For T = 134 °C (or lower than 134 °C) two elliptical patterns are observed in GISAXS data. Both scattering patterns are first-order Debye-Scherrer diffraction rings of the LAM structure in

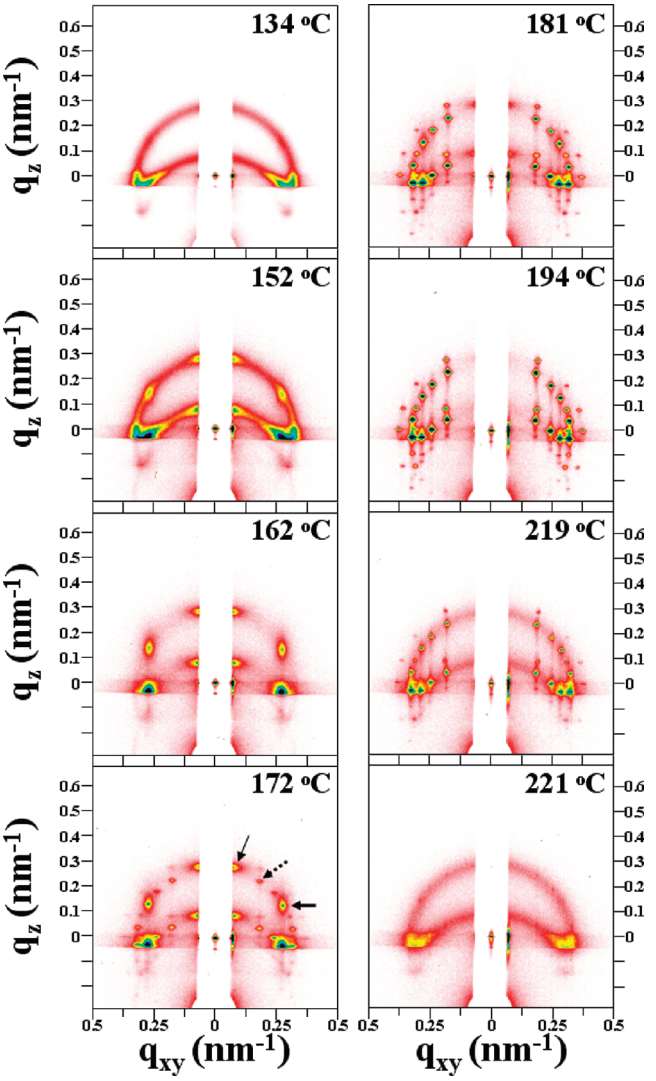

Figure 2. 2D GISAXS patterns for the film of 657 nm ($30L_0$) on PS grafted substrate at the incident angle of 0.18°, which is between the critical angle of the PS-*b*-PI film (0.134°) and the silicon substrate (0.198°). The patterns were taken during heating cycle from 100 to 222 °C at a rate of 0.5 °C/min for the thermally annealed film at 110 °C for 48 h under vacuum. Note that q values for axis labels are presented with respect to the reflected beam without a correction for refraction. Those in the main text are corrected for this. Detailed analysis on temperature dependence of SI-27 is performed for the three peaks pointed by arrows in the left bottom panel.

the film: The X-ray beam transmitting into the film produces the bottom ring, and the reflected beam off the substrate surface does the upper one. Since diffraction peaks by the reflected beam are always less distorted by the refraction effect,[41] we discuss BCP structures based on the peaks generated by the reflected beam throughout this work. During the analysis, however, all q_z components of diffraction peaks are corrected for the refraction of X-rays, and the values presented in the text of this paper are the corrected ones. Nevertheless, those rings indicate that the morphology at the low-temperature region is a randomly oriented LAM. As temperature increases to T = 162 °C, each ring is split into a set of peaks with a hexagonal symmetry, indicating a structure having a hexagonal arrangement in the plane normal to the X-ray beam. There is no higher-order peak except for the specular region along q_z axis, which suggests that only a short-range ordering exists along the in-plane direction while the film still possesses well-developed layered structure along the specular direction or the out-of-plane direction. Careful examination of

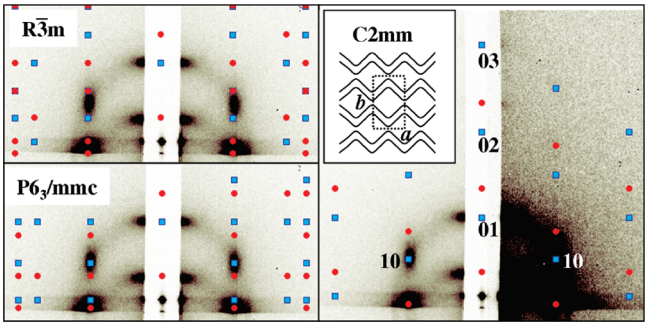

Figure 3. 2D GISAXS pattern observed for the film at 162 °C and peak indexing with three different space groups: $R\bar{3}m$ (HPL, ABCABC stacking), $P6_3/mmc$ (HCP, ABAB stacking), and *C*2*mm* (HML). Inset indicates the model of HML and its unit cell. Peaks are calculated with respect to the reflected (blue square) and transmitted (red circle) beams. Unit cell parameters of HML are 23.7 and 40.1 nm for *a* and *b*, respectively.

diffraction peaks along the q_z direction reveals that the even-order peaks are not observable. Indeed, the disappearance of the second-order peak in GISAXS indicates a mass shift of PS phase to PI sublayer, leading to the formation of a multibilayer structure with identical thicknesses. In modeling this structure, PL can be considered as a first guess because it was observed in the bulk sample. If perforated PS channels do not possess any ordering in the plane of a layer, there should not be any peak at the off-specular region. Therefore, the observation of the off-specular peaks in the GISAXS data as shown in Figure 3 suggests that the distance between perforated PS channels is well-defined, and thus their lateral size is so as well. If they are hexagonally arranged in a layer plane, the morphological structure would be either HPL or HCP. With both structures, however, we could not fit the observed peaks, as depicted in Figure 3. The other structure known to possibly exist during the transition between LAM to GYR is the hexagonally modulated lamella (HML).[15] In this case, the modulated structure is similar to the cylindrical structure (HEX) of BCPs in the sense that both perforated PS's of HML and cylinders of HEX are rodlike-shaped, and their long axes are hexagonally arranged. In fact, the GISAXS peaks are well fitted with 2D space group of *C*2*mm* that is a deformed 2D hexagonal as seen in the inset of Figure 3. The off-specular peaks correspond to the 10 peak of HEX, although we do not assign this structure as HEX because the SI-27 cannot form PI cylinders considering its volume fraction. As other perforated structures, the HML (*C*2*mm*) can also have identical thicknesses of the sublayers depending on the amplitude of modulations so that the disappearance of the second-order peak along the specular direction is explained by this model, too. With further increasing temperature up to T = 219 °C, the characteristic diffraction pattern of the GYR morphology appears. Finally at T = 221 °C, which is above the ODT temperature of the bulk by ~26 °C, all characteristic GYR peaks disappear and leave two broad elliptical rings, indicating a disordered state of the BCP film. For the SI-27 film, there is no indication of the *Fddd* structure throughout the temperature run. In summary, the SI-27 film shows the sequential OOT pathway composed of LAM-HML-GYR-DIS phases with increasing temperature, which is inconsistent with that of the bulk SI-27.

The position of primary peak (q^*) and its full width at half-maximum (fwhm) are plotted in Figure 4 as a function of temperature for the bulk (above) and the film (below) of SI-27. In GISAXS analysis, we focused on two first-order peaks: one (thick solid arrow in Figure 2 for T = 172 °C) in the off-specular region for tracking the in-plane structure and the other (thin solid arrow in Figure 2 for T = 172 °C) in the specular region to

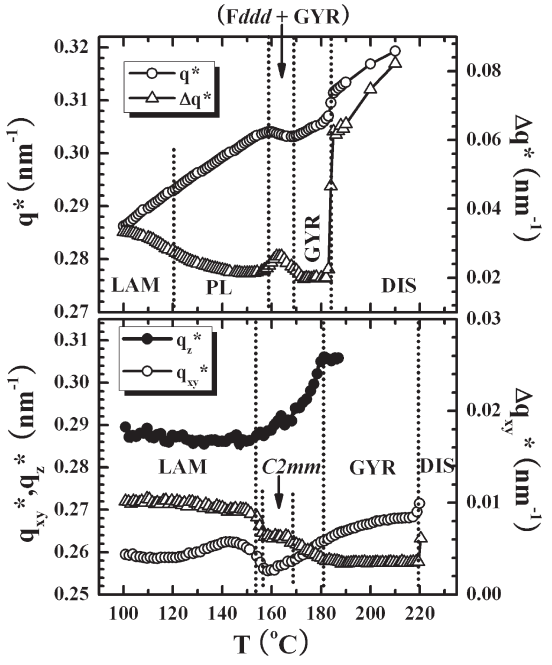

Figure 4. Temperature dependence of the positions of the primary peak q^* ($= 2\pi/d$) for the bulk (above) and film (below), which are derived from SAXS and GISAXS. For the bulk, q^* (○) and fwhm (△) denote the position of a primary peak and its width, respectively. The dotted lines indicate the transition temperatures such as OOT and ODT. For the film, q_{xy}^* (○) and its fwhm (△) are taken from a linecut at constant q_z = 0.134 nm^{-1} (indicated with a thick solid arrow in Figure 2). q_z^* (●) denotes the position of the primary peak along the specular region (indicated with a thin solid arrow in Figure 2), which is directly related to the interlayer *d*-spacing.

determine the layer *d*-spacing along the out-of-plane. In Figure 4 q_{xy}^* and q_z^* designate the q_{xy} component of the off-specular peak at q_z = 0.134 nm^{-1}, where the 01 peak of HML and 121 of GYR appear, and the q_z component of the specular peak, respectively.

In the bulk SI-27, the temperature ranges of LAM + PL, GYR, and DIS are clearly distinguishable; in general, q^* in the same morphology increases monotonously. The theory for the bulk BCP dictates the *d*-spacing $d \sim 2\pi/q^* \sim a(N^{2/3})(\chi^{1/6})$ in the regime of strong segregation limit (SSL), where *a* and *N* are the statistical segmental length and the number of monomer, respectively.[18] This is determined by the thermodynamic balance between the domain free energy (per chain) $F_{\mathrm{domain}}/kT \sim d^2/(a^2N)$ and interfacial energy (per chain) between two block components $F_{\mathrm{interface}}/kT \sim Na\chi^{1/2}/d$. Thus, the variation of *d*-spacing can be an indicator of conformational changes of the chains in the bulk BCP: two block chains stretched perpendicular to its domain interface will be relaxed with increasing temperature due to the decrease of χ parameter, which will result in the decrease of LAM *d*-spacing. The *d*-spacing can be also changed by the structural transformation such as perforation of PS to PI sublayer. As mentioned previously, we found a faster increase of q^* as a function of temperature than that of LAM in the literature,[14] which suggests that the PL is formed from the LAM structure. On the other hand, when a phase mixture *Fddd* + GYR is formed at T = 159−169 °C, q^* slightly decreases (or the increase of *d*-spacing) after it continuously increases through perforation to resolve the lattice mismatch issue. This rather striking phenomenon is related to the noncubic nature of *Fddd*: its first-order diffraction peak is the degeneration of three different peaks 111, 022, and 004. Since *Fddd* 022 has epitaxial relationship with LAM 001 and GYR 121, in an ideal case there may be no *d*-spacing change during the transition from PL to *Fddd* and *Fddd* to GYR transitions. When, however, the orthorhombic cell of *Fddd* is

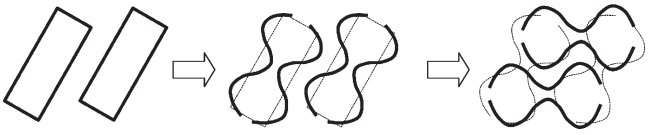

Figure 5. Possible structural transition mechanism from randomly oriented LAM to epitaxial HML.

slightly elongated, those three peaks could be splitted. Indeed, the fwhm of q^* on the formation of *Fddd* + GYR is increased as shown in Figure 4. Considering the epitaxial relationship, the peak that might appear at smaller q than q^* is probably 111. When LAM or PL is transformed to *Fddd*, *Fddd* 022 and 111 are originated from the out-of-plane and in-plane of lamella, respectively. Since the *d*-spacing is directly related to the conformation of BCP chains, slightly larger 111 may indicate more stretched BCP chains along the 111 direction that is parallel to the LAM or PL layer. Soon after, *Fddd* disappears at the same time when higher-order peaks of GYR are well developed, and then the *d*-spacing of GYR begins to decrease with increasing temperature. Eventually, a sharp discontinuity at higher temperature (184 °C) corresponds to ODT observed in the q^* plot.

For the film of SI-27, interesting observations in the transition from LAM to HML are the following: (1) the *d*-spacing of the interlayer distance of LAM that is parallel to the substrate does not decrease at all but slightly increases (or q_z^* decreases; denoted with filled dots in Figure 4) as a function of temperature. To reduce the layer *d*-spacing of LAM parallel to the substrate, BCP chains oriented normal to the substrate should slide away from each other in the in-plane so that stretched chains are relaxed toward Gaussain conformation, or their interchain distance should increase with increasing temperature, which corresponds to the decrease of χ parameter. When a polymer is incompressible, decreasing the layer *d*-spacing of LAM by 5% should increase the area of the film by about 5%, which will increase the surface energy and interfacial energy by that much. Thus, the energy gain obtained by not increasing the surface area compensates the decrease of the χ parameter. Of course, this argument only works for an epitaxially oriented LAM. For example, in the case of perpendicular LAM on a neutral substrate, the reduction of *d*-spacing will be facilitated, if the interfacial energy is not taken into account, because that could reduce the total surface area. In fact, we observed a decrease of the *d*-spacing for the LAM domain that is not parallel to the film (see the increase of q_{xy}^* in the LAM region in Figure 4). Thus, the contribution of surface and interfacial energies on the BCP chain conformation causes the *d*-spacing of parallel LAM increase with increasing temperature. The increase of the *d*-spacing of LAM (or slight decrease of q_z^*) may be partly due to the relaxation process of the shear thinned LAM. Please note that both q_z^* and q_{xy}^* of thin film LAM at 100 °C is slightly larger than q^* and $[(q^*)^2 - 0.134^2)]^{1/2}$ of bulk LAM, respectively.

(2) While LAM is randomly oriented on a substrate, HML is perfectly epitaxially oriented. Since rotations of LAM domains are hardly expected at the temperature range and in the time scale of this experiment, the transition from LAM to HML likely occurs through the undulation and rearrangement process,[42] as shown in the schematic drawing in Figure 5. The increase of q_z^* of HML as a function of temperature is notable in comparison to the slight decrease of q_z^* of LAM. The decrease of interlayer distance of HML is due to the increase of undulation with increasing temperature, as is found during the transition of LAM to PL in bulk. The drastic and continuous increase of q_z^* of HML may indicate that it is not an equilibrium structure considering the fact that those of LAM and GYR in the film are relatively insensitive to temperature in this work. In addition, such fast changes of q_{xy}^* and q_z^* upon a phase transition suggest

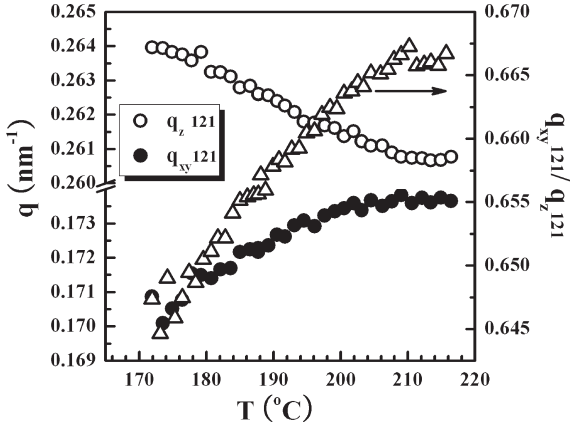

Figure 6. In-plane and out-of-plane q components of the GYR 121 diffraction peak that is indicated by a broken arrow in Figure 2, $q_{xy}121$ (●) and q_z121 (○), respectively, and their ratio, $q_{xy}121/q_z121$ (△).

that the higher OOT and ODT in the film compared to those in bulk occurs not because the dynamics of BCP chains is slow in the film but because the thermodynamic energy barrier such as surface/interfacial energy compensates for the reduction of the segregation power of BCP. As is for the bulk, fwhm of the q^* peak in the film is also sensitively changed upon an OOT but constant between the OOT's, indicating that a grain rearrangement or growth occurs only through OOT in the time frame used in this work.

Figure 6 shows two q components of the GYR 121 diffraction peak (indicated by the broken arrow in Figure 2); those are $q_{xy}121$ and q_z121 and their ratio of $q_{xy}121/q_z121$. When GYR is a perfect cubic, the ratio of $q_{xy}121/q_z121$ should be 0.6631. As is shown in the plot of $q_{xy}121/q_z121$, however, it is smaller than the ideal value at temperatures below 200 °C. Especially in the just-formed GYR at 180 °C *d*-spacing along the in-plane direction is about 2.3% larger than that along the out-of-plane. Since q_z^* of the GYR in the film at 180 °C, shown in Figure 4, is only about 0.5% larger than q^* of the GYR in bulk at the same temperature, one may say that the GYR in the film is stretched along the in-plane direction. This deformation in GYR is inherited from the HML. When a HML has a perfect hexagonal arrangement, the ratio of lattice parameters of *C2mm* shown in Figure 3 should be $a:b = 1:\sqrt{3}$. We, however, observed the ratio 1:1.692 for it, indicating that the HML in the film is a stretched hexagonal along the in-plane direction by about 2.3%. With increasing temperature GYR restores to a cubic: $q_{xy}121$ increases while q_z121 decreases, or *d*-spacings along the in-plane and out-of-plane decrease and increase, respectively. The surprising decrease of q_z121 of GYR (the increase of *d*-spacing along the out-of-plane) with increasing temperature is due to the force to restore the deformed structure to a cubic. Since an elastic force is getting weaker as a structure is being restored, the variation of $q_{xy}121$ and q_z121 become slower with increasing temperature while the mobility of BCP chains should be higher at higher temperature. As GYR becomes a perfect cubic, the temperature dependence of $q_{xy}121$ and q_z121 is significantly reduced as explained above, and finally GYR transformed to the isotropic disordered phase (DIS).

The modulus of PS-*b*-PI having M_n = 32 000 g/mol with the GYR morphology at 200 °C is around 1−10 GPa.[22] To deform *d*-spacing by 2.5%, the required force per a unit area (or energy per unit volume) is 25−250 k J/m^3. Surface tensions (or surface energy densities) of PS and PI are about 0.0435 and 0.032 J/m^2, respectively,[43] which correspond to 66 and 49 kJ/m^3 of energy densities for 657 nm thick film. Since the moduli of LAM and HML are smaller than that of GYR, the energy gain by wetting PS grafted substrate with PS block may be enough to deform

LAM and HML but not GYR. Additionally this explains why thicker film is less likely deformed and has a T_{ODT} closer to that in bulk.[36] The role of PI block of SI-27 in the deformation of the HML is less significant not only because it is a minor block but also it has relatively lower surface energy and modulus than those of the PS block. Consequently, the interfacial energy between the PS block of SI-27 and PS brushes on substrate is a dominating factor that deforms HML, which prohibits any increase of PS surface area and finally suppresses the compositional fluctuation of BCP. The OOT's without PL and *Fddd* and a higher T_{ODT} in the film are because the surface and interfacial energies do not allow the stretched BCP chains to relax. As soon as there is enough thermal energy to break the balance, OOT and ODT in the film occur as quickly as those in bulk does or even faster because the mobility of BCP chains at higher transition temperature is higher.

In conclusion, we studied morphological transitions in the bulk and film of an asymmetric PS-*b*-PI. The OOT pathway in bulk was LAM-PL-(*Fddd* + GYR)-GYR-DIS, where *Fddd* was poorly developed and coexists with developing GYR at the narrow temperature range. A transient morphology PL was observed between LAM and GYR in both bulk and film; the structure of the transient morphology in film was resolved better due to the preferential orientation and turned out to be HML. Another difference in the OOT pathway between in film and bulk is that *Fddd* was not found in the film. Finally, the OOT pathway in the film that preferentially interacts with a PS grafted substrate was LAM-HML-GYR-DIS. The microdomains in the film except DIS and LAM were preferentially oriented forming a layer structure parallel to the substrate. We found that in film morphological structures including GYR that is a cubic structure were stretched along the in-plane direction. Interestingly, the *d*-spacing of the parallel layers in film did not decrease at all in spite of the decrease of the segregation power of SI-27 with increasing temperature. It only decreased through the structural transition such as LAM to HML transition. The surface energy prohibiting the surface area expansion of the film and the interfacial energy preventing the formation of the PS-terminated surface on the PS-grafted substrate may be those that preferentially stabilize parallel LAM over the other orientations. They compensate for the decrease of the segregation power of BCP chains, especially for the chains normal to a substrate, and result in higher T_{OOT}'s and T_{ODT}. We observed that OOT and ODT in the film occur as quickly as those in bulk, suggesting that the dynamics of BCP chains in the film is not significantly slower than those in bulk and that the higher transition temperatures are not due to the kinetics or slow chain dynamics in film.

Acknowledgment. This work was supported by National Research Foundation (KRF-2008- D00297) and the Nuclear R&D Programs funded by the Ministry of Education, Science & Technology (MEST), Korea. The work at the Argonne National Laboratory was supported by U.S. Department of Energy, Office of Science, Office of Basic Energy Sciences, under Contract DE-AC02-06CH11357. B.L. thanks Dr. Myung Im Kim and Dr. Mikihito Takenaka for the comments and discussions on *Fddd*.

References and Notes

(1) Förster, S.; Antonietti, M. *Adv. Mater.* **1998**, *10* (3), 195–217.
(2) Discher, B. M.; Won, Y.; Ege, D. S.; Lee, J. C. M.; Bates, F. S.; Discher, D. E.; Hammer, D. A. *Science* **1999**, *284* (5417), 1143–1146.
(3) Zehner, R. W.; Sita, L. R. *Langmuir* **1999**, *15* (19), 6139–6141.
(4) Li, R. R.; Dapkus, P. D.; Thompson, M. E.; Jeong, W. G.; Harrison, C.; Chaikin, P. M.; Register, R. A.; Adamson, D. H. *Appl. Phys. Lett.* **2000**, *76* (13), 1689–1691.
(5) Thurn-Albrecht, T.; Schotter, J.; Kastle, G. A.; Emley, N.; Shibauchi, T.; Krusin-Elbaum, L.; Guarini, K.; Black, C. T.; Tuominen, M. T.; Russell, T. P. *Science* **2000**, *290* (5499), 2126–2129.
(6) Black, C. T.; Guarini, K. W.; Milkove, K. R.; Baker, S. M.; Russell, T. P.; Tuominen, M. T. *Appl. Phys. Lett.* **2001**, *79* (3), 409–411.
(7) Cheng, J. Y.; Ross, C. A.; Chan, V. Z. H.; Thomas, E. L.; Lammertink, R. G. H.; Vancso, G. J. *Adv. Mater.* **2001**, *13* (15), 1174–1178.
(8) Liu, K.; Baker, S. M.; Tuominen, M.; Russell, T. P.; Schuller, I. K. *Phys. Rev. B* **2001**, *63* (6), 060403.
(9) Lopes, W. A.; Jaeger, H. M. *Nature* **2001**, *414* (6865), 735–738.
(10) Shin, K.; Leach, K. A.; Goldbach, J. T.; Kim, D. H.; Jho, J. Y.; Tuominen, M.; Hawker, C. J.; Russell, T. P. *Nano Lett.* **2002**, *2* (9), 933–936.
(11) Ryu, D. Y.; Shin, K.; Drockenmuller, E.; Hawker, C. J.; Russell, T. P. *Science* **2005**, *308* (5719), 236–239.
(12) Yang, S. Y.; Park, J.; Yoon, J.; Ree, M.; Jang, S. K.; Kim, J. K. *Adv. Funct. Mater.* **2008**, *18* (9), 1371–1377.
(13) Jo, A.; Joo, W.; Jin, W.-H.; Nam, H.; Kim, J. K. *Nat. Nano* **2009**, *4* (11), 727–731.
(14) Tanaka, H.; Hashimoto, T. *Macromolecules* **1991**, *24* (20), 5713–5720.
(15) Hamley, I. W.; Koppi, K. A.; Rosedale, J. H.; Bates, F. S.; Almdal, K.; Mortensen, K. *Macromolecules* **1993**, *26* (22), 5959–5970.
(16) Spontak, R. J.; Smith, S. D.; Ashraf, A. *Macromolecules* **1993**, *26* (5), 956–962.
(17) Matsen, M. W.; Schick, M. *Phys. Rev. Lett.* **1994**, *72* (16), 2660.
(18) Matsen, M. W.; Bates, F. S. *Macromolecules* **1996**, *29* (4), 1091–1098.
(19) Hamley, I. W. C. V. *Prog. Polym. Sci.* **2004**, *29*, 909–948.
(20) Zhao, J.; Majumdar, B.; Schulz, M. F.; Bates, F. S.; Almdal, K.; Mortensen, K.; Hajduk, D. A.; Gruner, S. M. *Macromolecules* **1996**, *29* (4), 1204–1215.
(21) Schulz, M. F.; Khandpur, A. K.; Bates, F. S.; Almdal, K.; Mortensen, K.; Hajduk, D. A.; Gruner, S. M. *Macromolecules* **1996**, *29* (8), 2857–2867.
(22) Förster, S.; Khandpur, A. K.; Zhao, J.; Bates, F. S.; Hamley, I. W.; Ryan, A. J.; Bras, W. *Macromolecules* **1994**, *27* (23), 6922–6935.
(23) Khandpur, A. K.; Foerster, S.; Bates, F. S.; Hamley, I. W.; Ryan, A. J.; Bras, W.; Almdal, K.; Mortensen, K. *Macromolecules* **1995**, *28* (26), 8796–8806.
(24) Hajduk, D. A.; Harper, P. E.; Gruner, S. M.; Honeker, C. C.; Kim, G.; Thomas, E. L.; Fetters, L. J. *Macromolecules* **1994**, *27* (15), 4063–4075.
(25) Schulz, M. F.; Bates, F. S.; Almdal, K.; Mortensen, K. *Phys. Rev. Lett.* **1994**, *73* (1), 86.
(26) Avgeropoulos, A.; Dair, B. J.; Hadjichristidis, N.; Thomas, E. L. *Macromolecules* **1997**, *30* (19), 5634–5642.
(27) Vigild, M. E.; Almdal, K.; Mortensen, K.; Hamley, I. W.; Fairclough, J. P. A.; Ryan, A. J. *Macromolecules* **1998**, *31* (17), 5702–5716.
(28) Ahn, J.-H.; Zin, W.-C. *Macromolecules* **2000**, *33* (2), 641–644.
(29) Takenaka, M.; Wakada, T.; Akasaka, S.; Nishitsuji, S.; Saijo, K.; Shimizu, H.; Kim, M. I.; Hasegawa, H. *Macromolecules* **2007**, *40* (13), 4399–4402.
(30) Kim, M. I.; Wakada, T.; Akasaka, S.; Nishitsuji, S.; Saijo, K.; Hasegawa, H.; Ito, K.; Takenaka, M. *Macromolecules* **2008**, *41* (20), 7667–7670.
(31) Kim, M. I.; Wakada, T.; Akasaka, S.; Nishitsuji, S.; Saijo, K.; Hasegawa, H.; Ito, K.; Takenaka, M. *Macromolecules* **2009**, *42* (14), 5266–5271.
(32) Park, I.; Lee, B.; Ryu, J.; Im, K.; Yoon, J.; Ree, M.; Chang, T. *Macromolecules* **2005**, *38* (25), 10532–10536.
(33) Park, H.-W.; Im, K.; Chung, B.; Ree, M.; Chang, T.; Sawa, K.; Jinnai, H. *Macromolecules* **2007**, *40* (7), 2603–2605.
(34) Shin, C.; Ryu, D. Y.; Huh, J.; Kim, J. H.; Kim, K.-W. *Macromolecules* **2009**, *42* (6), 2157–2160.
(35) Matsen, M. W.; Bates, F. S. *Macromolecules* **1996**, *29* (23), 7641–7644.
(36) Shin, C.; Ahn, H.; Kim, E.; Ryu, D. Y.; Huh, J.; Kim, K.-W.; Russell, T. P. *Macromolecules* **2008**, *41* (23), 9140–9145.
(37) Kim, E.; Ahn, H.; Ryu, D. Y.; Kim, J.; Cho, J. *Macromolecules* **2009**, *42* (21), 8385–8391.
(38) Hajduk, D. A.; Ho, R.-M.; Hillmyer, M. A.; Bates, F. S.; Almdal, K. *J. Phys. Chem. B* **1998**, *102* (8), 1356–1363.
(39) Hamley, I. W.; Castelletto, V.; Mykhaylyk, O. O.; Yang, Z.; May, R. P.; Lyakhova, K. S.; Sevink, G. J. A.; Zvelindovsky, A. V. *Langmuir* **2004**, *20* (25), 10785–10790.
(40) Leibler, L. *Macromolecules* **1980**, *13* (6), 1602–1617.
(41) Lee, B.; Park, I.; Yoon, J.; Park, S.; Kim, J.; Kim, K.-W.; Chang, T.; Ree, M. *Macromolecules* **2005**, *38* (10), 4311–4323.
(42) Sakurai, S.; Aida, S.; Okamoto, S.; Sakurai, K.; Nomura, S. *Macromolecules* **2003**, *36* (6), 1930–1939.
(43) Dalnoki-Veress, K.; Forrest, J. A.; Stevens, J. R.; Dutcher, J. R. *J. Polym. Sci., Part B: Polym. Phys.* **1996**, *34* (17), 3017–3024.